**Atmospheric
Chemistry
and Physics
Discussions**

Improved simulation of group averaged CO$_2$ surface concentrations using GEOS-Chem and fluxes from VEGAS

Z. H. Chen[1], J. Zhu[2], and N. Zeng[3]

[1]International Center for Climate and Environment Science, Institute of Atmospheric Physics, Chinese Academy of Sciences, Beijing 100029, China
[2]State Key Laboratory of Atmospheric Boundary Layer Physics and Atmospheric Chemistry (LAPC), Institute of Atmospheric Physics, Chinese Academy of Sciences, Beijing 100029, China
[3]Department of Meteorology and Earth System Science Interdisciplinary Center, University of Maryland, College Park, MD 20742-2425, USA

Correspondence to: Z. H. Chen (czh@mail.iap.ac.cn), J. Zhu (jzhu@mail.iap.ac.cn), and N. Zeng (zeng@umd.edu)

Abstract

CO_2 measurements have been combined with simulated CO_2 distributions from a transport model in order to produce the optimal estimates of CO_2 surface fluxes in inverse modeling. However one persistent problem in using model-observation com-parisons for this goal relates to the issue of compatibility. Observations at a single site reflect all underlying processes of various scales that usually cannot be fully resolved by model simulations at the grid points nearest the site due to lack of spatial or tempo-ral resolution or missing processes in models. In this article we group site observations of multiple stations according to atmospheric mixing regimes and surface character-istics. The group averaged values of CO_2 concentration from model simulations and observations are used to evaluate the regional model results. Using the group aver-aged measurements of CO_2 reduces the noise of individual stations. The difference of group averaged values between observation and modeled results reflects the uncer-tainties of the large scale flux in the region where the grouped stations are. We com-pared the group averaged values between model results with two biospheric fluxes from the model Carnegie-Ames-Stanford-Approach (CASA) and VEgetation-Global-Atmosphere-Soil (VEGAS) and observations to evaluate the regional model results. Results show that the modeling group averaged values of CO_2 concentrations in all re-gions with fluxes from VEGAS have significant improvements for most regions. There is still large difference between two model results and observations for grouped average values in North Atlantic, Indian Ocean, and South Pacific Tropics. This implies possible large uncertainties in the fluxes there.

1 Introduction

An improved understanding of the carbon sources and sinks at a global scale is essen-tial to predict the future rate of atmospheric CO_2 increases and to plan an international CO_2 management strategy (Tans et al., 1990). But these fluxes remain quantitatively

uncertain. The full range of results in past studies spans budgets with northern terrestrial uptake of 0.5 to $4\,PgC\,yr^{-1}$, and tropical terrestrial emissions of -1 to $4\,PgC\,yr^{-1}$ (Stephens et al., 2007; Peylin et al., 2002; Gurney, 2004). Some studies show increasing sinks in tropical forest plots (Baker et al., 2004). Piao's results show that rising temperatures may already decrease the efficiency of terrestrial carbon uptake in the Northern Hemisphere (Piao et al., 2008), while larger net sinks were found over northern and southern continents (Feng et al., 2011).

It is not possible to measure all CO_2 sources and sinks in the every part of the globe. Fortunately any geographical distribution of CO_2 sources and sinks is reflected in the spatial and temporal variations of CO_2 concentration patterns in the atmosphere. The CO_2 in atmosphere is an unbribable witness of the surface flux. In early studies concentration differences between monitoring sites have been used as a constraint to infer net fluxes (Enting et al., 1995; Kaminski et al., 1998). The mean annual meridianal/longitudinal gradient observation is compared with model values (Bousquet et al., 1999; Kaminski et al., 1998). Latitudinal distribution of the sources and sinks of CO_2 from the concentration gradient has been discussed. The samples are grouped into latitude bands to derive the sources and sinks (Tans et al., 1989, 1990). Some inverse technique researches adjust the CO_2 surface flux via minimizing the distance between the modeled/optimized values and the observational data at each station (Enting, 2002; Peylin et al., 2002; Bousquet, 2000; Baker et al., 2006; Gurney et al., 2002; Rodenbeck et al., 2006).

However one persistent problem in using model-observation comparisons for this goal relates to the issue of compatibility. Observations at a single site reflect all underlying processes of all scales that usually cannot be fully resolved by model simulations at the grid points nearest the site due to lack of spatial or temporal resolution or missing processes in models. In this article we proposed a new technique to evaluate the regional surface fluxes by checking group averaged differences between model simulation and observations, rather than the difference at every single observational site. To compare and validate the climatological and yearly-varying CO_2 fluxes using the

modeled CO_2 results of GEOS-Chem model, several sites in one region are grouped according to the regional characteristics of temporal distribution of seasonal cycle derived from a new atmospheric CO_2 observation dataset from GLOBALVIEW-CO_2 2010. The difference of observation and modeled results of the average of stations in one group can reflect the uncertainties of the flux in the region where the grouped stations are.

Where and when the CO_2 emissions from fossil fuels are absorbed by land ecosystems and oceans is a major issue for global carbon cycle. It is significant for using highly accurate inventories in the optimization of CO_2 fluxes with inverse method. There are three parts which needed to be taken into account, emissions from fossil fuel, net ecosystem exchange of the terrestrial biosphere and ocean-atmosphere carbon exchange. Optimized estimates of surface source and sink are produced by some different bottom-up and top-down ways. GEOS-Chem atmospheric transport model has been widely used in the assimilation of CO_2 and inverse of CO_2 flux. It was used to evaluate the influence of reduced carbon emissions on the distribution of atmospheric CO_2 and described in early studies (Suntharalingam, 2004, 2005). Nassar made modifications to the GEOS-Chem CO_2 simulation including improved temporal variability in the national surface fossil fuel inventory, the addition of surface CO_2 shipping, 3-D domestic and international aviation CO_2 emissions, and 3-D chemical production of CO_2 (Nassar et al., 2010). The balanced biosphere flux is based on a 3-h NEP for 2000 from CASA model (Olsen, 2004), which has always been used as the prior flux in the GEOS-Chem. It is available for the simulation of global CO_2 concentration using new net land-atmosphere carbon exchange with the development of Dynamic Global Vegetation Model (DGVM). The spatial trends in Net Biome Production (NBP) have been produced by different DGVMs (http://www-lscedods.cea.fr/invsat/RECCAP/V2/Data% 20Policy%20Trendy.pdf).

All DGVMs are consistent with the global land carbon budget (Sitch et al., 2008). VEGAS model is developed to simulate the net primary productivity and described by Zeng (Zeng et al., 2005; Zeng, 2003). In this paper the land-atmosphere fluxes from

VEGAS is introduced into GEOS-Chem model to replace all the current inventories except fossil and ocean flux.

The outline of this paper is as follows: Sect. 2 introduces the data. Section 3 of this paper group observation stations in one region and demonstrate the temporal and spatial variability in CO_2. Section 4 presents the group averaged differences between the observation and the model results with fluxes from CASA (VEGAS). We present conclusions in Sect. 5.

2 Data

2.1 GLOBALVIEW CO_2 data

GLOBALVIEW-CO_2 (GLOBALVIEW-CO2, 2010) is an update product of the Cooperative Atmospheric Data Integration Project. While the project is coordinated and maintained by the Carbon Cycle Greenhouse Gases Group of the National Oceanic and Atmospheric Administration, Earth System Research Laboratory (NOAA ESRL), gaps in the data are filled by extrapolation from marine boundary layer measurements. Flask samples of whole air enable highly accurate and precise measurements of atmospheric CO_2 concentrations (Conway et al., 1994). It can be downloaded from http://www.esrl.noaa.gov/gmd/ccgg/globalview/co2/co2_download.html. This update includes extended records derived from observation made by 21 laboratories from 14 countries. The data product includes extended records for the period 1 January 1979 to 1 January 2010. We choose one lowest record if there are several records at different altitude for the same site, and 108 records are kept. For one record, the negative value denotes the smoothed value of CO_2 concentration in this month is less than the benchmark trend values.

2.2 VEGAS data

Net ecosystem exchange (NEE, which = net primary productivity (NPP) – heterotrophic respiration (RH)) is simulated by DGVMs. Simulated land-atmosphere fluxes are between -1.52 and $-2.75\,\mathrm{Pg\,C\,yr^{-1}}$ for the 1990s, DGVMs simulate a greater land carbon uptake, which is in agreement with IPCC estimates (Sitch et al., 2008). The land fluxes are defined as the sum of photosynthesis, ecosystem respiration and biomass burning. The terrestrial carbon model VEGAS is described in Zeng (2003). It was run at $2.5° \times 2.5°$ resolution and forced by the observed precipitation and temperature. The monthly NBP flux as net land-atmosphere carbon exchange is regridded offline to the GEOS grids ($2° \times 2.5°$) in this work, which is equal to the magnitude of NEE.

A diurnally varying NEP flux is constructed from gross primary production (GPP) and ecosystem respiration (Re) in the CASA model (Olsen, 2004). The CASA NEP output is used as NEE in GEOS-Chem. The comparisons of monthly land-atmosphere fluxes from VEGAS and CASA are concluded as Fig. 1. The difference of spatial distribution is seen as Fig. 2 (January) and Fig. 3 (July). It is evident that the largest sinks in July of VEGAS is smaller than that of CASA about 500 Tg, which is distributed in the region of Asia, South America boreal, and South American tropical. The sources of VEGAS from January to April is lower than that of CASA, which is distributed in the region of South American tropical and Northern Africa.

The original emission inventories (ORI) in GEOS-Chem is shown in Fig. 1, which includes the balanced biosphere from CASA, biofuel burning, biomass burning and residual annual biospheric flux (Nassar et al., 2010) and is replaced with fluxes from VEGAS in this work. Obviously the sinks of VEGAS are smaller than the original results in GEOS-Chem especially from June to August. The summary of fluxes is in Appendix A.

3 Grouped CO$_2$ observations

3.1 Determining groups of observational sites

To represent the regional characteristics of CO$_2$, several stations are grouped according to the regional characteristics of temporal distribution of seasonal cycle. The stations are grouped based on two factors: atmospheric mixing regimes and surface characteristics (land or ocean). Atmospheric mixing regimes can be reflected by seasonal pattern and amplitude of the seasonal trends of each station.

All groups in land show similar patterns. The minimum value of CO$_2$ appears in summer and fall, and the maximum value appears in spring and winter. The difference between minimum and maximum values is much more than 6 ppm for most stations in land. The Earth was divided into 11 land and 11 ocean regions in TransCom3 project (Gurney et al., 2002). The 11 TransCom land regions are used except the boundary of two land regions. The latitude is defined as the division for most two adjacent land regions in this work. The stations in each land region are grouped.

The differences of seasonal pattern and amplitude of stations in Ocean regions are apparent. We group the stations in ocean regions as follows: The stations that have similar phase and magnitude range are grouped. We also require that all the sites in one group should be next to each other in order to approximately reflect the same type of sink/source. Then the ocean is divided into 15 regions and the stations in Ocean regions are grouped to 15 groups. All 108 stations (see Table A1) are classified into 26 groups and 72 sites in 15 ocean regions. The map of all grouped sites is shown in Fig. 4.

3.2 Seasonal patterns of stations in land regions

All groups in the land show a similar pattern. The seasonal patterns of stations (more than one station) in 5 regions are shown in Fig. 5. We can know that the minimum value for land groups appears in summer and fall, and the maximum value appears

in spring and winter from Fig. 5. Seasonal cycles of atmospheric CO_2 are caused primarily by the terrestrial biosphere moving from being a net source of carbon to the atmosphere (mainly in winter) to becoming a net sink (mainly in summer), where net carbon uptake or release is determined by the balance between photosynthesis and respiration. Seasonal cycle of atmospheric CO_2 in the Northern Hemisphere (NH) is in phase with the ecosystems (Randerson et al., 1997). The difference of the magnitude for the amplitude, minimum values, maximum values of all groups in the NH can be an important constraint for further improving our understanding of the surface fluxes in the NH.

3.3 Seasonal patterns of stations in ocean regions

The ocean was divided into 15 regions based on the seasonal trends of CO_2, including Pacific Ocean region (O1–O7), Atlantic regions (O8–O11), Indian regions (O12–O13), Northern Ocean (O14), and Southern Ocean (O15).

The stations in the Pacific Ocean North of 5° S are classified into 5 different groups (O1, O2, O3, O6 and O7), and the stations in the Atlantic Ocean are classified into 2 groups (O8, O9). Though the seasonal trends of ocean regions north of 5° S are similar as that of the land groups in Northern Hemisphere, there are different amplitudes as shown in Fig. 6. The amplitude of groups O1, O6 is larger than 10 ppm, and the amplitude of O2, O7 is much less than that of northern regions, while the amplitude of group O3 is much less than 6 ppm. The amplitude of group O9 is less than that of group O8. The amplitude typically decreases moving southward, since the Southern Hemisphere has less mid-latitude vegetation to seasonally absorb and release CO_2 (Randerson et al., 1997). We require that all the sites in one group should be next to each other in order to approximately reflect the same type of sink/source. To separate these regions with different amplitudes of concentration of CO_2, it is helpful to distinguish when and where the sources and sinks are.

The South Pacific region between 5° S and 35° S is divided into two subregions (O4 and O5) according to the different seasonal trend of stations in these regions. Though

the amplitude is smaller than 1.4 ppm, the seasonal patterns of the groups are clear in these regions. The sites in South Pacific region between 5° S and 15° S (group O4) show a special trend. The minimum appears in September or October. There are two obvious increase phases from April to June and from October to December, which indicate that there may be sources in these months. The sites of group O5 locate in South Pacific region between 15° S and 35° S shows another special trend, the maximum value of group O5 appears in January, the minimal value appears in May, which indicates there may be sinks from January to May and from June to September in this region.

The seasonal patterns are more complicated in the Indian Ocean South of 35° S. They are classified into two groups with different seasonal patterns (O12 and O13). The average pattern is totally different from other oceans. The North Indian Ocean O12 shows a consistent decrease from February to November. The stations in South Indian Ocean O13 show chaos in the first half year and show a consistent increase in the second half year. The South Atlantic is divided into 2 regions (O10, O11) without average pattern, one station with quite different seasonal pattern in each region.

The concentrations of CO_2 of stations in ocean south of 5° S are mainly influenced by the oceanic sources and sinks, and the amplitudes of seasonal cycles are not more than 2 ppm (O4, O5, O10, O11, O15), which are much smaller than that of the NH. General negative values in seasonal cycle denote sinks, positive values denote sources. It is evident that the seasonal variations are positive in NH winter (January) and negative in NH summer (August). The seasonal variations are positive in austral winter (August) and negative in austral summer (January) in the south of 35° S, such as group O15 (Fig. 6). Seasonal signals observed in all subtropical regions of the NH and SH show that the CO_2 concentration decreases southward in summer and vice versa in winter (Metzl et al., 2006). Group O15 exhibits obvious increase from February to September and decrease from September to February in the next year. It is opposite in shape to that of NH; on the other hand, there are sources in austral winter and sinks in austral summer, which is similar as that of NH. To some extent, it is coherent for the whole

global in winter or summer. The seasonal variations typically decrease from positive to negative values from NH to SH in January, and increases from negative to positive values in August.

4   Simulation results and comparison with observations

We use the GEOS-Chem model (http://acmg.seas.harvard.edu/geos) to describe the relationship between 3-D atmospheric CO_2 concentrations and surface CO_2 fluxes. We carried out the simulations with original emission inventories (ori) and new emission inventories (new). CO_2 was simulated at a horizontal resolution of 2° latitude × 2.5° longitude with original emission inventories including CO_2 fluxes from fossil fuel combustion F_{ff}, biomass/biofuel burning F_{bb}, CASA balanced biosphere diurnal fluxes (Net Ecosystem Productivity for 2000) F_{nep}, residual annual terrestrial exchange F_{net}, ocean flux F_{oc}. A detail description of the emission inventories is given in Nassar et al. (2010). 375 ppm for 1 January 2004 is set for a starting point of spin-up. Then all inventories except fossil fuels F_{ff} and ocean flux F_{oc} were replaced with fluxes from VEGAS. A 7-day average timeseries of the model result with original inventories (dotted line in Figs. 7, 8) and new inventories for 2006 (dashed line in Figs. 7, 8) was compared with observations (real line in Figs. 7, 8).

4.1   Comparisons of group averaged CO_2 concentrations for land regions

The CO_2 seasonal patterns and amplitudes simulated by model runs with two emission inventories were different. The largest discrepancy between model results and observations for runs with original emission inventories is 17.5 ppm, about 4.5 % of observation values. The discrepancy for runs with new emission inventories is below 8.4 ppm, about 2.2 %. The largest discrepancies for both runs appear in the region L11, which indicates there may be large uncertainties for CO_2 surface fluxes in Europe.

The model results with new emission inventories have smaller discrepancy than the simulations with original emission inventories for North American boreal (L1) from January to September, which is smaller than 1 % of observations. It's higher than observations about 2–5 ppm from December to November, which suggests that more sinks in
5 North America may be required for this period.

There are good agreements between model results with new emission inventories and observations for North American Temperate and Eurasian boreal and Eurasian Temperate region (L2, L7 and L8). The biggest discrepancy is 4.4 ppm, 1.1 % of observations, which appears in December and better than the results with original emis-
10 sion inventories of 7.2 ppm for region L2. The largest discrepancy is decreased from 15.0 ppm to 4.4 ppm for region L7 by using the new emission inventories. The discrepancy is below 3.8 ppm for runs with new emission inventories, while 8.9 ppm for runs with original emission inventories in region L8.

The modeling results can not be compared with observations because of scarcity of
15 observations for South America, Africa, and Australia. The new emission inventories can be used as good prior fluxes in the forward model and be adjusted in future inverse model from the above comparisons of 5 land regions.

4.2   Comparisons of group averaged CO_2 concentrations for ocean regions

The trends of CO_2 concentration over ocean regions are also influenced by the change
20 of emission inventories in land. The largest discrepancy in ocean regions between the model results with new inventories and observations is below 7.8 ppm, 2.1 % of observations, which is lower than the discrepancy of results from original inventories (14.3 ppm). There are great improvements in the region south of 15° S (O5 and O11) for the model results with new inventories. It can be deduced that the sources and sinks
25 are improved in the South American Temperate though there is no direct observations in this region.

The largest discrepancy for runs with new inventories appears in April for Indian Tropical (O12). It has a persisting decrease from April for the observation, while there is

a minimum value in April for both model results. Both model results have discrepancy from January to April for South Indian Temperate (O13). It is very complex for the seasonal trend of the observation stations in South Indian Temperate. Unfortunately there is scarce of observations in the adjacent land regions. Some more observations
5 are very necessary for these regions in future.

There is still large positive bias for North Atlantic Temperate (O8, O9) from July to September. More sinks may be required in this region or the surrounded land region. It's difficult to simulate the concentration of South Pacific Tropics (O4), which has more complex seasonal cycles compared to other regions (Fig. 6). It is obviously that the
10 ocean emission inventories are needed to be adjusted to match the observations in the ocean region. In future work, the net land and ocean fluxes will be improved based on the discrepancy of the group averaged values between model results and observations.

4.3 Comparisons of the root-mean-square difference

To further demonstrate the difference of regional model results between original bio-
15 spheric fluxes (includes land-atmosphere fluxes from CASA) and new biospheric fluxes from VEGAS, we compare the root-mean-square difference (RMSD) between modeled and observed concentration at the observation sites in one group along with the group averaged values (Fig. 9). The RMSD of group averaged value between model results with fluxes from VEGAS and observation is reduced by 0.24–0.63 ppm for 5 land re-
20 gions.

The concentrations of CO_2 in ocean regions are influenced by the change of emission inventories in land. It is clear that the RMSD of group averaged value between model results using fluxes from VEGAS and observation is less than the results using fluxes from CASA by 0.15–0.53 ppm for North East Pacific, South Pacific and Southern
25 Ocean (O1, O4, O5, O12, O13 and O15). There is little improvement for North Pacific and Northern Ocean (O2, O6, and O14). It is convenient to evaluate the regional model results according to the comparisons of group averaged values.

5 Conclusions

We grouped several sites in one region according to the phase and amplitude of seasonal cycles of observations. The group averaged measurement values of CO_2 concentration contain less small scale "noise" that models often cannot resolve and are used to evaluate the regional model results. The differences of group averaged values between observations and model results reflect the uncertainties of the flux in the region where the grouped stations are.

We compared group averaged values between model results with two land-atmosphere flux from CASA (VEGAS) and observations. Results show that the modeling group averaged values of CO_2 concentrations with fluxes from VEGAS have improvements in most regions. There is still large uncertainty in Atlantic and North Atlantic, Indian Ocean, and South Pacific Tropics. This implies possible large uncertainties in the fluxes there.

The differences of group averaged values between observations and model results will be used to estimate the error of regional fluxes and optimize the regional fluxes with inversing methods in future work.

Appendix A

Summery of emission inventory

The original (new) CO_2 flux used in this study is 7.8 PgC (7.8 PgC, fossil emission inventories), −1.4 PgC (−1.4 PgC, net air-sea fluxes), −2.3 PgC (−1.9 PgC, net air-land fluxes) for 2006. The original(new) global annual net CO_2 emissions for 2006 is 4.1 PgC (4.5 PgC). The simulated seasonal cycles shows big discrepancies though there is a small difference between the total net fluxes from new emission inventories and original emission inventories in GEOS-Chem. There are also little differences between the total fluxes from other inversion results. JENA S99V3.2 data (3.78 PgC) is available

from http://www.bgc-jena.mpg.de/~christian.roedenbeck/download-CO2/; LSCE V1.0 (3.43 PgC) (Chevallier et al., 2010) is available from http://www.carboscope.eu/; Carbon Tracker-2009 (4.15 PgC) is available from http://www.esrl.noaa.gov/gmd/ccgg/carbontracker/; and two inversion results (4.1 PgC, 4.7 PgC) are from (Feng et al., 2011; Nassar et al., 2011).

It is hard to evaluate the inverse results by the total value. It's very useful to compare the group averaged values using these inventories to evaluate inverse results in future work.

References

Baker, D. F., Law, R. M., Gurney, K. R., Rayner, P., Peylin, P., Denning, A. S., Bousquet, P., Bruhwiler, L., Chen, Y. H., Ciais, P., Fung, I. Y., Heimann, M., John, J., Maki, T., Maksyutov, S., Masarie, K., Prather, M., Pak, B., Taguchi, S., and Zhu, Z.: TransCom 3 inversion intercomparison: Impact of transport model errors on the interannual variability of regional CO_2 fluxes, 1988–2003, Global Biogeochem. Cy., 20, GB1002, doi:10.1029/2004GB002439, 2006.

Baker, T. R., Phillips, O. L., Malhi, Y., Almeida, S., Arroyo, L., Di Fiore, A., Erwin, T., Higuchi, N., Killeen, T. J., and Laurance, S. G.: Increasing biomass in Amazonian forest plots, Philos. Trans. Roy. Soc. London B, 359, 353, 2004.

Bousquet, P.: Regional changes in carbon dioxide fluxes of land and oceans since 1980, Science, 290, 1342–1346, doi:10.1126/science.290.5495.1342, 2000.

Bousquet, P., Ciais, P., Peylin, P., Ramonet, M., and Monfray, P.: Inverse modeling of annual atmospheric CO_2 sources and sinks 1. Method and control inversion, J. Geophys. Res., 104, 26161–26178, 1999.

Chevallier, F., Ciais, P., Conway, T., Aalto, T., Anderson, B., Bousquet, P., Brunke, E., Ciattaglia, L., Esaki, Y., and Fröhlich, M.: CO_2 surface fluxes at grid point scale estimated from a global 21 year reanalysis of atmospheric measurements, J. Geophys. Res., 115, D21307, 2010.

Title Page

Abstract | Introduction

Conclusions | References

Tables | Figures

◄ | ►►

◄ | ►

Back | Close

Full Screen / Esc

Printer-friendly Version

Interactive Discussion

Conway, T., Tans, P., Waterman, L., Thoning, K., Kitzis, D., Masarie, K., and Zhang, N.: Evidence for interannual variability of the carbon cycle from the NOAA/CMDL global air sampling network, J. Geophys. Res, 99, 22831–22855, 1994.

Enting, I., Trudinger, C., and Francey, R.: A synthesis inversion of the concentration and δ^{13} C of atmospheric CO_2, Tellus B, 47, 35–52, 1995.

Enting, I. G.: Inverse Problems in Atmospheric Constituent Transport, Cambridge University Press, Cambridge, 2002.

Feng, L., Palmer, P. I., Yang, Y., Yantosca, R. M., Kawa, S. R., Paris, J.-D., Matsueda, H., and Machida, T.: Evaluating a 3-D transport model of atmospheric CO_2 using ground-based, aircraft, and space-borne data, Atmos. Chem. Phys., 11, 2789–2803, doi:10.5194/acp-11-2789-2011, 2011.

GLOBALVIEW-CO_2: Cooperative Atmospheric Data Integration Project – Carbon Dioxide, NOAA ESRL, Boulder, CO, 2010.

Gurney, K. R.: Transcom 3 inversion intercomparison: Model mean results for the estimation of seasonal carbon sources and sinks, Global Biogeochem. Cy., 18, Gb1010, doi:10.1029/2003gb002111, 2004.

Gurney, K. R., Law, R. M., Denning, A. S., Rayner, P. J., Baker, D., Bousquet, P., Bruhwiler, L., Chen, Y. H., Ciais, P., and Fan, S.: Towards robust regional estimates of CO_2 sources and sinks using atmospheric transport models, Nature, 415, 626–630, 2002.

Kaminski, T., Heimann, M., Giering, R., and fur Meteorologie, M. P. I.: A global scale Inversion of the transport of CO_2 based on a matrix representation of an atmospheric transport model derived by its adjoint, Air Pollut. Model. Appl., XII, 247, 1998.

Metzl, N., Brunet, C., Jabaudjan, A., Poisson, A., and Schauer, B.: Summer and winter air–sea CO_2 fluxes in the Southern Ocean, Deep-Sea Res. Pt. I, 53, 1548–1563, doi:10.1016/j.dsr.2006.07.006, 2006.

Nassar, R., Jones, D. B. A., Suntharalingam, P., Chen, J. M., Andres, R. J., Wecht, K. J., Yantosca, R. M., Kulawik, S. S., Bowman, K. W., Worden, J. R., Machida, T., and Matsueda, H.: Modeling global atmospheric CO_2 with improved emission inventories and CO_2 production from the oxidation of other carbon species, Geosci. Model Dev., 3, 689–716, doi:10.5194/gmd-3-689-2010, 2010.

Nassar, R., Jones, D. B. A., Kulawik, S. S., Worden, J. R., Bowman, K. W., Andres, R. J., Suntharalingam, P., Chen, J. M., Brenninkmeijer, C. A. M., Schuck, T. J., Conway, T. J., and Worthy, D. E.: Inverse modeling of CO_2 sources and sinks using satellite observations

of CO$_2$ from TES and surface flask measurements, Atmos. Chem. Phys., 11, 6029–6047, doi:10.5194/acp-11-6029-2011, 2011.

Olsen, S. C.: Differences between surface and column atmospheric CO$_2$ and implications for carbon cycle research, J. Geophys. Res., 109, D02301, doi:10.1029/2003jd003968, 2004.

5 Peylin, P., Baker, D., Sarmiento, J., Ciais, P., and Bousquet, P.: Influence of transport uncertainty on annual mean and seasonal inversions of atmospheric CO$_2$ data, J. Geophys. Res, 107, 4385, doi:10.1029/2001JD000857, 2002.

Piao, S., Ciais, P., Friedlingstein, P., Peylin, P., Reichstein, M., Luyssaert, S., Margolis, H., Fang, J., Barr, A., Chen, A., Grelle, A., Hollinger, D. Y., Laurila, T., Lindroth, A., Richard-

10 son, A. D., and Vesala, T.: Net carbon dioxide losses of northern ecosystems in response to autumn warming, Nature, 451, 49–52, doi:10.1038/nature06444, 2008.

Randerson, J. T., Thompson, M. V., Conway, T. J., Fung, I. Y., and Field, C. B.: The contribution of terrestrial sources and sinks to trends in the seasonal cycle of atmospheric carbon dioxide, Global Biogeochem. Cy., 11, 535–560, 1997.

15 Rödenbeck, C., Conway, T. J., and Langenfelds, R. L.: The effect of systematic measurement errors on atmospheric CO$_2$ inversions: a quantitative assessment, Atmos. Chem. Phys., 6, 149–161, doi:10.5194/acp-6-149-2006, 2006.

Sitch, S., Huntingford, C., Gedney, N., Levy, P., Lomas, M., Piao, S., Betts, R., Ciais, P., Cox, P., and Friedlingstein, P.: Evaluation of the terrestrial carbon cycle, future plant geography and

20 climate–carbon cycle feedbacks using five Dynamic Global Vegetation Models (DGVMs), Glob. Change Biol., 14, 2015–2039, 2008.

Stephens, B. B., Gurney, K. R., Tans, P. P., Sweeney, C., Peters, W., Bruhwiler, L., Ciais, P., Ramonet, M., Bousquet, P., and Nakazawa, T.: Weak northern and strong tropical land carbon uptake from vertical profiles of atmospheric CO$_2$, Science, 316, 1732, 2007.

25 Suntharalingam, P.: Improved quantification of Chinese carbon fluxes using CO$_2$/CO correlations in Asian outflow, J. Geophys. Res., 109, D18S18, doi:10.1029/2003jd004362, 2004.

Suntharalingam, P.: Influence of reduced carbon emissions and oxidation on the distribution of atmospheric CO$_2$: implications for inversion analyses, Global Biogeochem. Cy., 19, GB4003, doi:10.1029/2005gb002466, 2005.

30 Tans, P. P., Conway, T. J., and Nakazawa, T.: Latitudinal distribution of the sources and sinks of atmospheric carbon dioxide derived from surface observations and an atmospheric transport model, J. Geophys. Res., 94, 5151–5172, 1989.

Title Page

Abstract | Introduction

Conclusions | References

Tables | Figures

◄ | ►

Back | Close

Full Screen / Esc

Printer-friendly Version

Interactive Discussion

Tans, P. P., Fung, I. Y., and Takahashi, T.: Observational constraints on the global atmospheric CO_2 budget, Science, 247, 1431–1438, 1990.

Zeng, N.: Glacial-interglacial atmospheric CO_2 change – the glacial burial hypothesis, Adv. Atmos. Sci., 20, 677–693, 2003.

5   Zeng, N., Mariotti, A., and Wetzel, P.: Terrestrial mechanisms of interannual CO_2 variability, Global Biogeochem. Cy., 19, GB1016, doi:10.1029/2004GB002273, 2005.

Improved simulation of group averaged

Z. H. Chen et al.

Title Page

Abstract   Introduction

Conclusions   References

Tables   Figures

◄   ►

Back   Close

Full Screen / Esc

Printer-friendly Version

Interactive Discussion

Table A1. Stations used in this paper.

station_name	Longtitude	Latitude	Height	Group
cba_01D0	−162.72	55.2	25	O1
csj_06D0	−131.02	51.93	89	O1
esp005_01P2	−126.55	49.38	500	O1
ljo_04D0	−117.3	32.9	10	O1
pocn35_01D1	−143	35	10	O1
pocn40_01D1	−138	40	10	O1
pocn45_01D1	−131	45	10	O1
pta_01D0	−123.73	38.95	17	O1
stp_12D0	−145	50	7	O1
thd005_01P2	−124.15	41.05	500	O1
haa005_01P2	−158.95	21.23	500	O2
kum_01D0	−154.82	19.52	3	O2
mid_01D0	−177.38	28.21	4	O2
pocn10_01D1	−152	10	10	O2
pocn15_01D1	−147	15	10	O2
pocn20_01D1	−140	20	10	O2
pocn25_01D1	−134	25	10	O2
pocn30_01D1	−126	30	10	O2
chr_01D0	−157.17	1.7	3	O3
poc000_01D1	−163	0	10	O3
pocn05_01D1	−158	5	10	O3
pocs05_01D1	−168	−5	10	O3
pocs10_01D1	−174	−10	10	O4
pocs15_01D1	−178	−15	10	O4
smo_01C0	−170.57	−14.24	42	O4
eic_01D0	−109.45	−27.15	50	O5
pocs20_01D1	−178.5	−20	10	O5
pocs25_01D1	174	−25	10	O5
pocs30_01D1	169	−30	10	O5
rta005_01P2	−159.83	−21.25	500	O5
coi_20C0	145.5	43.15	100	O6
gsn_24D0	126.15	33.28	72	O6
shm_01D0	174.1	52.72	40	O6
tap_01D0	126.13	36.73	20	O6
gmi_01D0	144.78	13.43	2	O7
hat_20C0	123.8	24.05	47	O7

Improved simulation of group averaged

Z. H. Chen et al.

Title Page

Abstract	Introduction
Conclusions	References
Tables	Figures

◄ | ►

◄ | ►

Back | Close

Full Screen / Esc

Printer-friendly Version

Interactive Discussion

Table A1. (Continued).

station_name	Longtitude	Latitude	Height	Group
mnm_19C0	153.97	24.3	8	O7
scsn06_01D1	107	6	15	O7
scsn09_01D1	109	9	15	O7
scsn12_01D1	111	12	15	O7
scsn15_01D1	113	15	15	O7
scsn18_01D1	115	18	15	O7
scsn21_01D1	117	21	15	O7
yon_19C0	123.02	24.47	30	O7
azr_01D0	−27.38	38.77	40	O8
bme_01D0	−64.65	32.37	30	O8
avi_01D0	−64.75	17.75	3	O9
izo_01D0	−16.48	28.3	2360	O9
key_01D0	−80.2	25.67	3	O9
rpb_01D0	−59.43	13.17	45	O9
asc_01D0	−14.42	−7.92	54	O10
cpt_36C0	18.49	−34.35	260	O11
cri_02D0	73.83	15.08	60	O12
daa_02D0	130.57	−12.42	3	O13
sey_01D0	55.17	−4.67	3	O13
trm_11D0	54.52	−15.88	20	O13
alt_01D0	−62.52	82.45	210	O14
ice_01D0	−20.29	63.34	118	O14
mbc_01D0	−119.35	76.25	58	O14
sis_02D0	−1.17	60.17	30	O14
stm_01D0	2	66	5	O14
wes_23C0	8	55	8	O14
zep_01D0	11.88	78.9	475	O14
aia005_02D2	144.3	−40.53	500	O15
crz_01D0	51.85	−46.45	120	O15
cya_02D0	110.52	−66.28	2	O15
hba_01D0	−26.5	−75.58	30	O15
jbn_29C0	−58.82	−62.23	15	O15
maa_02D0	62.87	−67.62	32	O15
mqa_02D0	158.97	−54.48	12	O15
psa_01D0	−64	−64.92	10	O15
syo_01D0	39.58	−69	11	O15

Table A1. (Continued).

station_name	Longtitude	Latitude	Height	Group
amt012_01C3	−68.68	45.03	62	L1
brw_01C0	−156.6	71.32	11	L1
cdl030_06C3	−105.12	53.99	630	L1
cmo_01D0	−123.97	45.48	30	L1
dnd010_01P2	−97.77	48.38	1000	L1
egb_06C0	−79.78	44.23	226	L1
fsd040_06C0	−81.57	49.88	250	L1
hfm005_01P2	−72.17	42.54	500	L1
lef010_01P2	−90.27	45.93	1000	L1
llb010_06C3	−112.45	54.95	550	L1
nha005_01P2	−70.63	42.95	500	L1
opw_01D0	−124.42	48.25	488	L1
pfa015_01P2	−147.29	65.07	1500	L1
bao022_01C3	−105.01	40.05	1606	L2
bne010_01P2	−97.18	40.8	1000	L2
hdpdta_03C0	−111.65	40.56	3369	L2
hil010_01P2	−87.91	40.07	1000	L2
itn051_01C3	−77.38	35.35	60	L2
sgp374_01D0	−97.48	36.62	688	L2
spldta_03C0	−106.73	40.45	3219	L2
wbi010_01P2	−91.35	41.72	1000	L2
wkt030_01C3	−97.62	31.32	281	L2
kzd_01D0	75.57	44.45	412	L7
kzm_01D0	77.88	43.25	2519	L7
uum_01D0	111.1	44.45	914	L7
ryo_19C0	141.83	39.03	260	L8
wlg_01D0	100.9	36.29	3810	L8
bal_01D1	17.22	55.35	28	L11
bsc_01D0	28.68	44.17	3	L11
cmn_17C0	10.7	44.18	2165	L11
hpb_01D0	11.01	47.8	985	L11
mhd_01D0	−9.9	53.33	25	L11
orl005_11D2	2.5	47.8	500	L11
pal_01D0	24.12	67.97	560	L11
pdm_11D0	0.13	42.93	2877	L11
sch_23C0	8	48	1205	L11

Improved simulation of group averaged

Z. H. Chen et al.

Title Page

Abstract	Introduction
Conclusions	References
Tables	Figures

◀ ▶

◀ ▶

Back Close

Full Screen / Esc

Printer-friendly Version

Interactive Discussion

Full Screen / Esc

Printer-friendly Version

Interactive Discussion
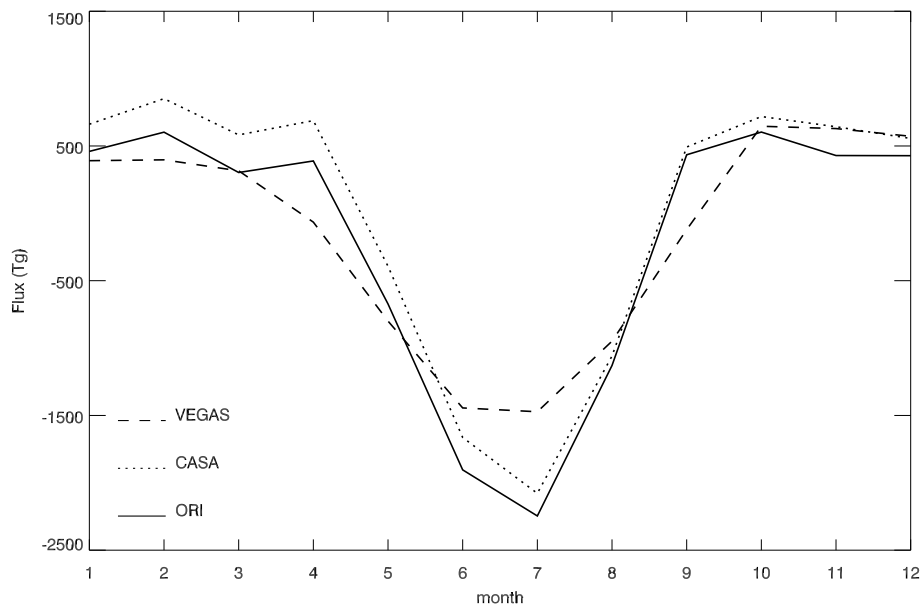
Fig. 1. Monthly terrestrial fluxes from dynamic global vegetation models (CASA and VEGAS) and original land-atmosphere fluxes (ORI, including fluxes from CASA, biofuel burning, biomass burning and residual annual biospheric flux) in GEOS-Chem in 2006.
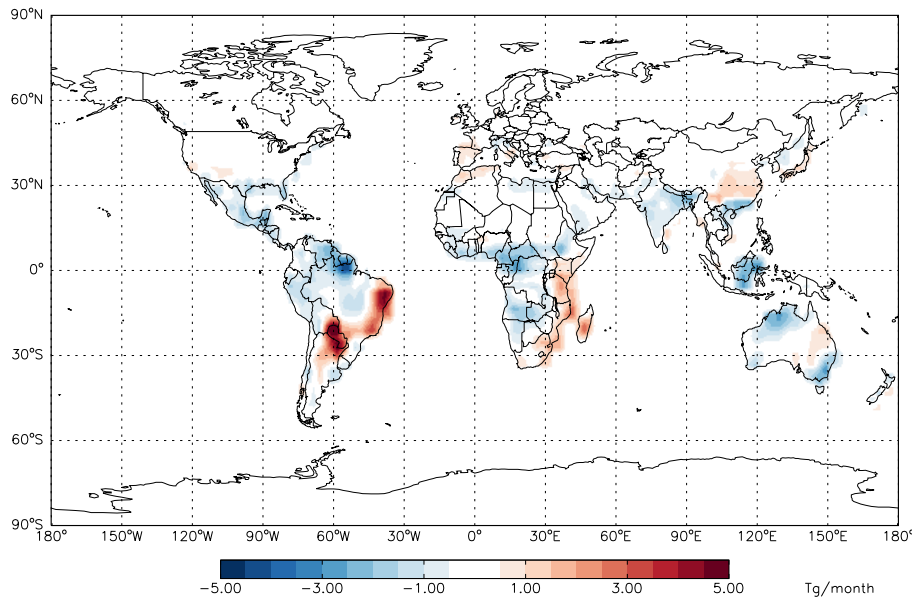
Fig. 2. Spatial distribution of difference between terrestrial exchange from CASA and fluxes from VEGAS in January 2006 (positive values denote the fluxes from VEGAS are greater than the fluxes from CASA).

Full Screen / Esc

Printer-friendly Version

Interactive Discussion
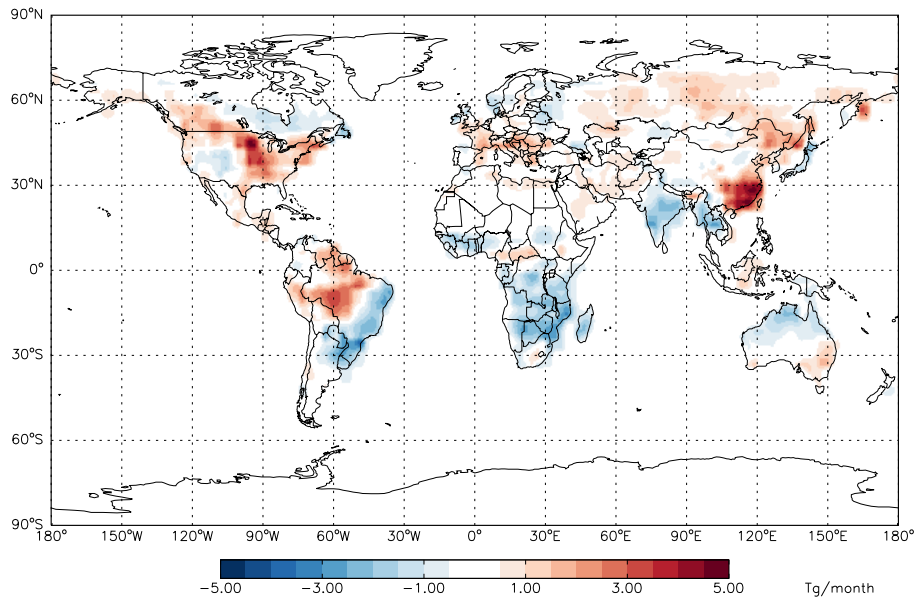
Fig. 3. Difference of spatial distribution between terrestrial exchange from CASA and fluxes from VEGAS in July 2006.
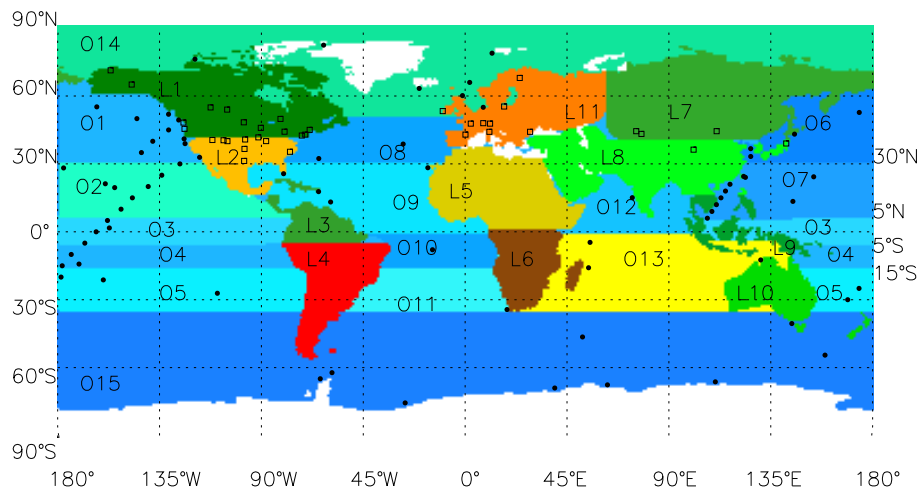
Fig. 4. The locations of the observing stations (72 sites in ocean (closed circle), 36 sites in land (open square)), and the regions over the globe (15 ocean regions and 11 land regions). The stations in one region are grouped. The ocean is divided into 15 regions and the stations in Ocean regions are grouped to 15 groups. The land is divided into 11 regions and the stations in land regions are grouped to 11 groups. (L1: North American boreal, L2: North American Temperate, L3: South American Tropical, L4: South American Temperate, L5: Northern Africa, L6: Southern Africa, L7: Eurasian boreal, L8: Eurasian Temperate, L9: Tropical Asia, L10: Australia, L11: Europe, O1: North East Pacific, O2: North East Pacific Temperate, O3: Pacific Tropics, O4: South Pacific Tropics, O5: South Pacific Temperate, O6: North West Pacific, O7: North West Pacific Temperate, O8: North Atlantic, O9: North Atlantic Temperate, O10: Atlantic Tropics, O11: South Atlantic Temperate, O12: Indian Tropical, O13: South Indian Temperate, O14: Northern Ocean, O15: Southern Ocean).
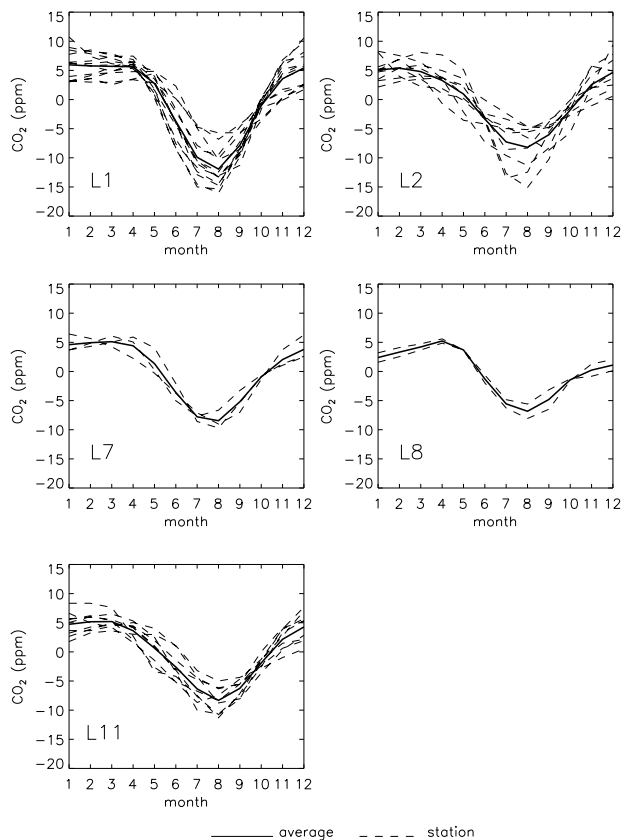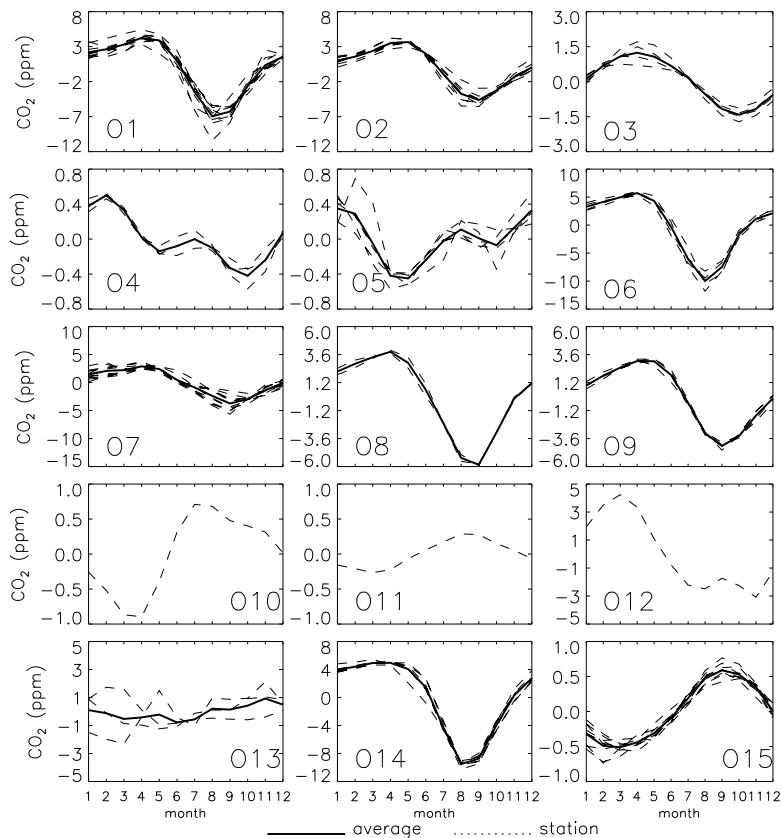
Fig. 5. Seasonal cycles of observational stations in 5 land groups in land regions where there are more than 2 stations (5 regions are shown in Fig. 4, broken line denotes the seasonal values for all stations in one region, real line denotes the grouped average value of each region).

ACPD

13, 2243–2271, 2013

Improved simulation of group averaged

Z. H. Chen et al.

Title Page

Abstract | Introduction

Conclusions | References

Tables | Figures

◄ | ►

◄ | ►

Back | Close

Full Screen / Esc

Printer-friendly Version

Interactive Discussion

Fig. 6. Seasonal cycles of observational stations of 15 ocean groups in ocean regions (15 regions are shown in Fig. 4, broken line denotes the seasonal values for all stations in one region, real line denotes the group averaged value of each region).
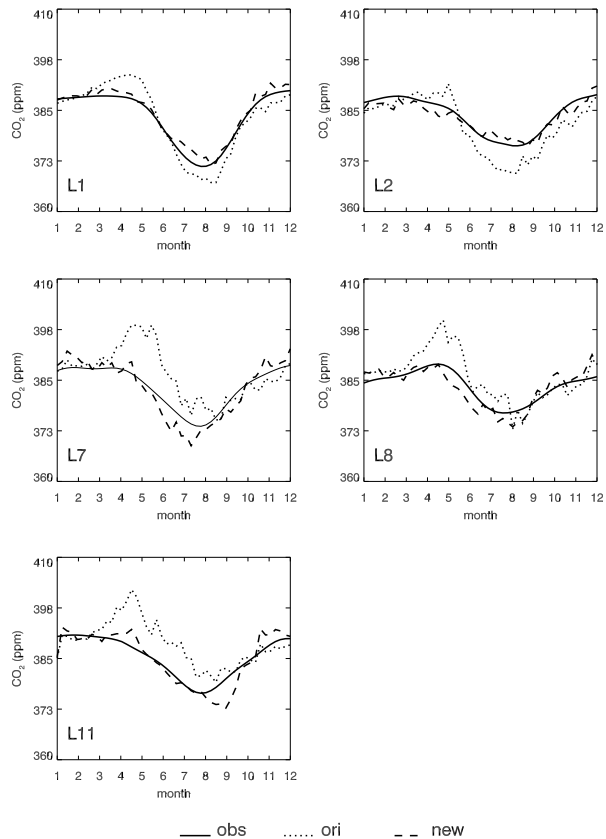
Fig. 7. Comparisons of group averaged values of CO_2 between model results from GEOS-Chem with original emission inventories (dotted line) and new emission inventories (dashed line) and GLOBALVIEW-CO_2 (real line) for 5 land regions in 2006 (5 regions are shown in Fig. 4).

Discussion Paper | Discussion Paper | Discussion Paper | Discussion Paper |

ACPD

13, 2243–2271, 2013

Improved simulation of group averaged

Z. H. Chen et al.

Title Page

Abstract | Introduction

Conclusions | References

Tables | Figures
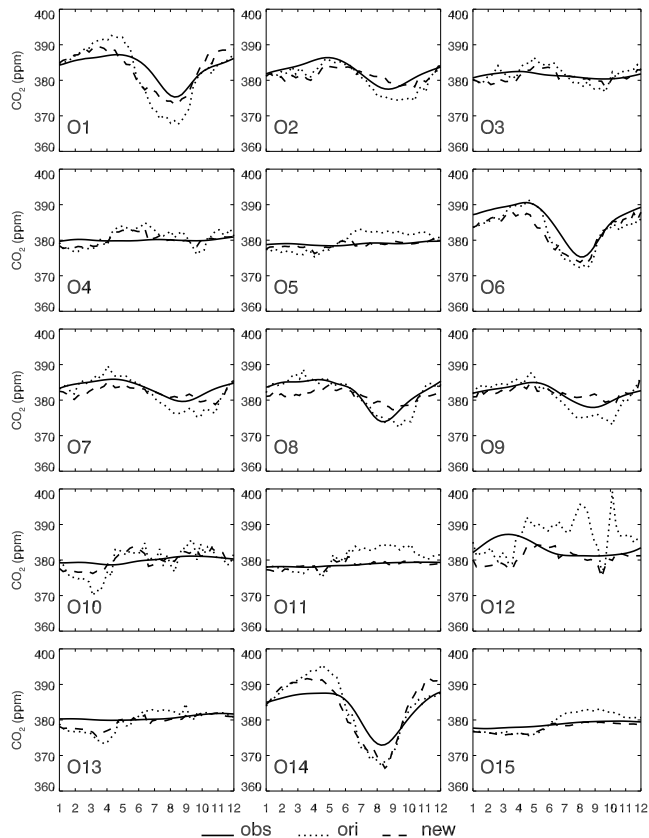
|◄ | ►|

◄ | ►

Back | Close

Full Screen / Esc

Printer-friendly Version

Interactive Discussion

Fig. 8. Comparisons of group averaged values of CO_2 between model results from GEOS-Chem with original emission inventories (dotted line) and new emission inventories (dashed line) and GLOBALVIEW-CO_2 (real line) for 15 ocean regions (15 ocean regions are shown in Fig. 4).

Discussion Paper | Discussion Paper | Discussion Paper | Discussion Paper |

ACPD

13, 2243–2271, 2013

Improved simulation of group averaged

Z. H. Chen et al.

Title Page

Abstract | Introduction

Conclusions | References

Tables | Figures
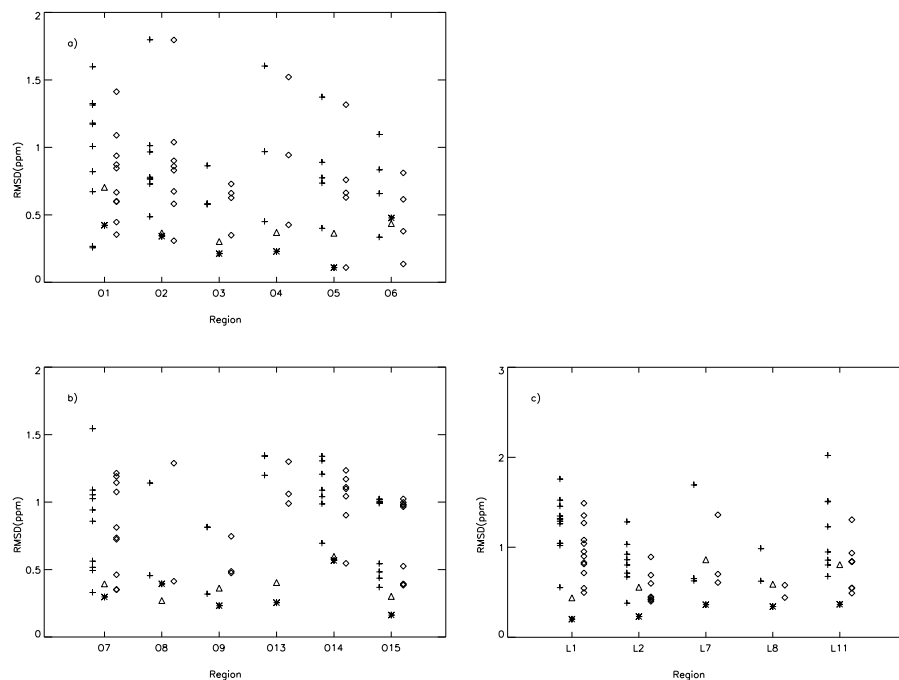
◀ | ▶|

◀ | ▶

Back | Close

Full Screen / Esc

Printer-friendly Version

Interactive Discussion

Fig. 9. Comparison of RMSD of each stations and group averaged values between model results and observations **(a)** Ocean regions in Pacific **(b)** other Ocean regions. **(c)** Land regions. Each region is shown in Fig. 4. Triangle (Asterisk) denotes RMSD of group averaged values between model results using fluxes from CASA (VEGAS) and observations, cross (diamond) denotes RMSD of each station between model results using fluxes from CASA (VEGAS) and observations.